This article has been accepted for publication in a future issue of this journal, but has not been fully edited. Content may change prior to final publication. Citation information: DOI 10.1109/LWC.2021.3132458, IEEE Wireless Communications Letters

Model-free radio map estimation in massive MIMO systems via semi-parametric Gaussian regression

Nicolò Dal Fabbro*⋆, Michele Rossi*‡, Gianluigi Pillonetto*, Luca Schenato*, Giuseppe Piro†§

***Abstract*—Accurate radio maps will be very much needed to provide environmental awareness and effectively manage future wireless networks. Most of the research so far has focused on developing power mapping algorithms for single and omnidirectional antenna systems. In this letter, we investigate the construction of crowdsourcing-based radio maps for 5G cellular systems with massive directional antenna arrays (spatial multiplexing), proposing an original technique based on semi-parametric Gaussian regression. The proposed method is *model-free* and provides highly accurate estimates of the radio maps, outperforming fully parametric and non-parametric solutions.**

***Index Terms*—REM, massive MIMO, 5G**

I. Introduction

A radio environment map (REM) is a database of communication quality metrics (CQMs). In cellular systems, REMs associate geographical user positions with the CQMs of interest. Designed as intelligent units attached to the existing network infrastructure, REMs will play a key role in the resource management of future cellular networks. Indeed, they will allow boosting the performance of wireless systems by providing average radio channel quality information for, e. g., predictive resource allocation [1], handover optimization [2], and energy efficient designs [3]. CQMs vary with the user position and the adopted frequency band [4]. Furthermore, REMs need to be updated through time [5], [6]. For these reasons, and given the poor accuracy of REMs built upon empirical path loss models [4], [5], measurement-based approaches have been extensively investigated. These approaches consist in either deploying an ad hoc wireless sensor network [7] or in crowdsourcing CQMs from mobile users [4]. Spatial interpolation techniques like Gaussian process regression (or Kriging) [8] are typically applied to predict CQM values in unmeasured locations. The majority of the works in the literature have focused on radio power mapping in systems with omnidirectional antennas [7], [9], [10], where the main objective of the estimation is the mean field, determined by the path loss (PL), together with the shadowing process. Notable exceptions considering directional antennas are [11], where the directional antenna model is parameterized, and [12], where the directive antenna radiation pattern is reconstructed. 5G cellular systems are characterized by the use of multiple-input multiple-output (MIMO) antenna arrays to increase transmission speed and efficiency [13]. In MIMO systems the spatial distribution of CQMs is dramatically influenced by antenna array configurations and transmission techniques, like spatial division multiplexing. Also, antenna arrays are subject to production imperfections and impairments [14] with many consequences such as beam directivity errors [15]. Non-ideal phenomena like mutual coupling can produce significant changes in the desired antenna beam shapes [16]. Moreover, practical working conditions of antenna arrays in cellular systems involve partial faults in the antenna emitting capabilities, due to the typical characteristics of the outdoor environment where a base station (BS) is placed, causing distortions in the generated beams [17], [18]. Hence, relying on the antenna array model to capture the array impact on the REM could introduce an unreliable bias. These issues motivate the study of a model-free solution for the REM estimation in MIMO systems. In this letter, we address the problem of crowdsourcing-based Signal to Interference plus Noise Ratio (SINR) radio map construction in a massive MIMO (mMIMO) sector (256 transmitting antennas) with grid-of-beams (GoB), under Joint Spatial Division and Multiplexing (JSDM), in sub-6GHz bands. In this setup, the spatial multiplexing determined by spatial directional beams generated by large antenna arrays at the transmitter has a major impact on the radio map. To the best of our knowledge, no work in the literature has so far addressed the problem of crowdsourcing-based REM construction in a mMIMO cellular system, and this is the first work proposing a strategy to jointly estimate the combined effect of the GoB-based mMIMO transmission technology and of environmental attenuation (PL and shadowing) in the REM computation. We propose a model-free measurement-based regression strategy to jointly estimate the mean field - related to the generated GoB and PL - and the shadowing process. The proposed approach falls in the framework of semi-parametric Gaussian Process regression, but, differently from baseline solutions, the proposed estimator captures the GoB impact on the REM via the design of an ad hoc parametric space. In particular, parametric spaces spanned by Fourier bases [19] and Chebyshev polynomials [20] are experimented with, assessing their capability of representing the GoB structure.

The hyperparameters learning and map reconstruction performance of the proposed REM estimation method are evaluated through intensive simulations using advanced channel models, compliant with the 5G new radio standard, under

This work has received funding from the Italian Ministry of Education, University and Research (MIUR) through the PRIN project no. 2017NS9FEY entitled "Realtime Control of 5G Wireless Networks: Taming the Complexity of Future Transmission and Computation Challenges"

⋆Corresponding author.

*Department of Information Engineering (DEI), University of Padova, via Gradenigo 6/b, 35131, Padova, Italy. (e-mail: {name.surname}@dei.unipd.it)

†Department of Electrical and Information Engineering (DEI), via Orabona, 4 - 70125, Bari, Italy (e-mail: giuseppe.piro@poliba.it)

‡Department of Mathematics "Tullio Levi-Civita", via Trieste 63, 35131, Padova, Italy.

§CNIT, Consorzio Nazionale Interuniversitario per le Telecomunicazioni, Pisa, Italy

different antenna array configurations.

Notation: Vectors and matrices are written as lower and upper case bold letters, respectively (e.g., vector $\mathbf{v}$ and matrix $\mathbf{V}$). $\mathbf{V}^T$, $|\mathbf{V}|$ and $(\mathbf{V})_{i,j}$ denote $\mathbf{V}$'s transpose, determinant and (i, j) entry, respectively. $\mathbf{I}$ denotes an identity matrix, $\mathbf{0}$ a vector of zeros, $\mathbb{E}[.]$ the expectation operator.

II. System overview

We consider a scenario with three-sectors base stations (BSs) serving adjacent cells. BSs are equipped with $M = 256$ antennas and we focus on an operating bandwidth of 25MHz composed of $B = 25$ consecutive sub-channels. Specifically, $\mathcal{B} = \{f_0, f_1, ..., f_{B-1}\}$ represents the set of sub-channels. Each BS is transmitting $T_l = 2$ spatially multiplexed layers through $n = 16$ or $n = 32$ beams. Mobile devices have $N_r = 2$ antennas. We consider a BS located at the origin of the Cartesian reference system. A mobile device located at position $\mathbf{x} \in \mathbb{R}^2$ receives, in the time-slot t_j, a signal $\mathbf{r}(\mathbf{x}, f_i, t_j) \in \mathbb{C}^{N_r \times 1}$ through its N_r antennas [21]:

$$\mathbf{r}(\mathbf{x}, f_i, t_j) = \sum_{l=1}^{L} \mathbf{H}_l(\mathbf{x}, f_i, t_j)\sqrt{\mathbf{Q}_l}\mathbf{V}_l(f_i, t_j)\mathbf{s}_l + \mathbf{n}, \quad (1)$$

where, $\mathbf{s}_l \in \mathbb{C}^{T_l}$ is the symbol transmitted by the l-th BS, $\mathbf{H}_l(\mathbf{x}, f_i, t_j) \in \mathbb{C}^{N_r \times M}$ is the channel matrix between the l-th BS and the considered device for sub-channel $f_i \in \mathcal{B}$, $\mathbf{Q}_l \in \mathbb{R}^{M \times M}$ is a diagonal power allocation matrix, $\mathbf{V}_l(f_i) \in \mathbb{C}^{M \times T_l}$ represents the downlink precoding matrix of the l-th BS for sub-channel $f_i \in \mathcal{B}$, and $\mathbf{n} \sim \mathcal{CN}\left(\mathbf{0}, \sigma^2\mathbf{I}\right)$ describes the Gaussian distributed uncorrelated noise with variance σ^2. Note that (1) also includes the interference contributions from within and across sectors [21]. The mMIMO JSDM scheme [21] implements a 2-stage precoding. In particular, the precoding matrix $\mathbf{V}_l(f_i, t_i)$ is split into two matrices

$$\mathbf{V}_l(f_i, t_i) = \mathbf{G}_l\mathbf{C}_l(f_i, t_i). \quad (2)$$

The 1-stage precoding matrix, $\mathbf{G}_l \in \mathbb{C}^{M \times n}$, realizes the GoB layout, where n independent signals, namely "the beams", are sent in a number of fixed spatial directions spanning the entire area of a cell sector. The 2-stage precoding matrix $\mathbf{C}_l(f_i, t_i) \in \mathbb{C}^{n \times T_l}$, instead, is configured by the BS to dynamically adapt the transmission power to the channel quality experienced by the mobile device. During network operation, $\mathbf{C}_l(f_i, t_i)$ is adapted to the available CSI on a sub-channel and time-slot basis, thus related to the small-scale fading (fast fading) effect. The matrix $\mathbf{H}_l(\mathbf{x}, f_i, t_j)$ describes the quality of the communication channel established between the BS l and the mobile device. The coefficients of such matrix specify the loss affecting the signal transmitted by an antenna of BS l and an antenna of the considered mobile device. That loss is modeled as the sum of three different propagation phenomena: path loss (PL), shadowing, and fast fading.

We choose the average effective SINR experienced by a user located in position $\mathbf{x}$, and denoted by $\gamma(\mathbf{x})$, as the REM channel quality metric (CQM) to be estimated, in the operating bandwidth of interest. Considering a long enough observation period and averaging over several sub-channels, the fast fading effect is averaged out (see, e.g., [4], [6]–[8]). As a consequence, even though the 2-stage precoding matrix $\mathbf{C}_l$ changes during network operation on a sub-channel and time-slot basis, compensating for the fast fading effect, this does not affect the average spatial process in the operating bandwidth of interest, which is the REM estimation target. The CQM $\gamma(\mathbf{x})$ is thus related to both the GoB layout generated by the mMIMO transmission technology, determined by the 1-stage precoding matrix, $\mathbf{G}_l$, and by the environmental attenuation (path loss and shadowing). To compute $\gamma(\mathbf{x})$ from the simulated channel, we adopt the Mutual Information Effective SINR Mapping (MIESM) method [22]. In this way, we get the effective SINR over the set of considered sub-channels $\mathcal{B}$, that we average both in frequency and time, over an observation period of adequate length (3s were used for our results).

We generate the REM via computer simulations, considering a spatial grid with a resolution of 1 square meter. Regarding the propagation model, an Urban Macro-cell IMT scenario with outdoor users is considered. The PL is modeled according to the M.2135 model [23]. The fast fading is modeled through pre-computed traces generated according to [24]. The shadowing is also simulated based on the same 3GPP specification. In Fig. 2-(a), we show the outcome of a simulation run: the impact of the spatial power distribution due to the GoB technique is evident from the power patterns.

III. Estimation method

We represent the spatial process of the average effective SINR $\gamma(\mathbf{x})$ as a random field in the two-dimensional space. In what follows, spatial functions are expressed in the dB domain. We have

$$\gamma(\mathbf{x}) = \mu(\mathbf{x}) + \delta(\mathbf{x}), \quad (3)$$

where $\mu(\mathbf{x})$ denotes the mean field and $\delta(\mathbf{x})$ is the so-called residual process, both functions of the position $\mathbf{x} \in \mathcal{X} = \mathbb{R}^2$.

For the map estimation, we decide to consider the residual process $\delta(\mathbf{x})$ to represent the shadowing process, that in the dB domain is usually modeled (see, e.g., [8]) as a Gaussian process ($\mathcal{GP}$) with positive semidefinite covariance $K : \mathcal{X} \times \mathcal{X} \to \mathbb{R}$, then we have $\gamma(\mathbf{x}) \sim \mathcal{GP}(\mu(\mathbf{x}), K(\mathbf{x}, \mathbf{x}'))$. The GoB effect and the path loss, instead, are represented by the mean field $\mu(\mathbf{x})$.

A. Regression

The regression consists in jointly estimating the mean field and the shadowing process. To apply the regression all the hyperparameters of the systems are required: in Section III-C we illustrate the learning strategies that we adopt. The shadowing is modeled as a Gaussian process (see [8]) with covariance function

$$K(\mathbf{x}, \mathbf{x}') = \lambda^2 \cdot \exp\left(-\frac{\|\mathbf{x} - \mathbf{x}'\|}{d_c}\right),$$

where d_c is the shadowing correlation distance and λ^2 is the process variance. The mean $\mu(\mathbf{x})$ of the process in (3) is here modeled as a linear combination of m basis functions defined on the space domain,

$$\mu(\mathbf{x}) = \sum_{k=1}^{m} w_k\phi_k(\mathbf{x}), \quad \{\phi_k : \mathcal{X} \to \mathbb{R}\}_{k=1}^{m}. \quad (4)$$

We consider a dataset $\mathcal{D} = \{\mathbf{x}_i, y_i\}_{i=1}^{N}$ of N crowd-sourced measurements $y_1, ..., y_N$ collected at spatial positions

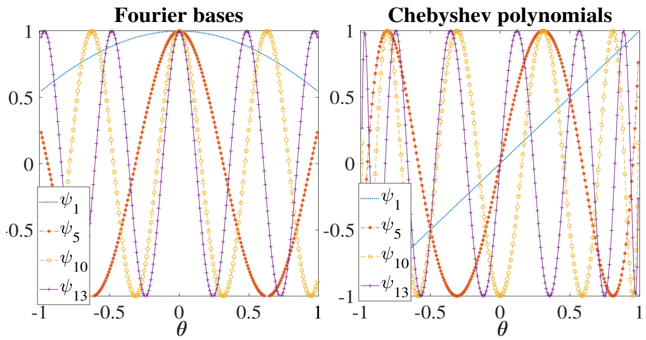

Fig. 1: Sets of used basis functions: Fourier bases and Chebyshev polynomials.

$\mathbf{x}_1, ..., \mathbf{x}_N$. In what follows, $\mathbf{y} = [y_1, ..., y_N]^T$. We consider the standard measurement model $y_i = \gamma(\mathbf{x}_i) + \epsilon_i$, where $\boldsymbol{\epsilon} \sim \mathcal{N}(\mathbf{0}, \sigma^2\mathbf{I})$, $\boldsymbol{\epsilon} = [\epsilon_1, ..., \epsilon_N]^T$. Given a well defined kernel function $K(\mathbf{x}, \mathbf{x}')$ associated with a map $\gamma(\mathbf{x})$ with mean $\mu(\mathbf{x})$ (see (4)), it is well known (see [25], [26]) that the optimal least-squares measurement-based estimate of the process in position $\mathbf{x}$ is

$$\hat{\gamma}(\mathbf{x}) = \sum_{i=1}^{N} \hat{c}_i K_{\mathbf{x}_i}(\mathbf{x}) + \sum_{k=1}^{m} \hat{w}_k \phi_k(\mathbf{x}), \tag{5}$$

where $K_{\mathbf{x}_i}(\mathbf{x}) = K(\mathbf{x}_i, \mathbf{x})$, and, defining $\hat{\mathbf{w}} := [\hat{w}_1, ..., \hat{w}_m]^T$ and $\hat{\mathbf{c}} = [\hat{c}_1, ..., \hat{c}_N]^T$, the optimal coefficients are as follows,

$$\hat{\mathbf{w}} = (\boldsymbol{\Phi}^T \mathbf{A}^{-1} \boldsymbol{\Phi})^{-1} \boldsymbol{\Phi}^T \mathbf{A}^{-1} \mathbf{y}, \tag{6}$$

$$\hat{\mathbf{c}} = \mathbf{A}^{-1}(\mathbf{y} - \boldsymbol{\Phi}\hat{\mathbf{w}}), \tag{7}$$

$$(\bar{\mathbf{K}})_{i,j} = K(\mathbf{x}_i, \mathbf{x}_j), \quad \mathbf{A} = \bar{\mathbf{K}} + \sigma^2\mathbf{I}, \quad (\boldsymbol{\Phi})_{i,j} = \phi_j(\mathbf{x}_i). \tag{8}$$

With respect to equation (5), a *fully parametric* estimator would use only a linear combination of the basis functions $\phi_k(\mathbf{x})$, while a *fully non-parametric* estimator only linear combinations of the kernel sections, $K_{\mathbf{x}_i}(\mathbf{x})$.

B. Parametric space for GoB estimation

The mMIMO JSDM scheme strongly impacts the radio map because of the many directional beams emitted in different angular directions producing the GoB configuration. Given this symmetric peculiarity of the GoB impact on the REM, we introduce a parametric space made up of bases that, considering a reference system with origin corresponding to the BS location, are functions of the angular variable. Considering for convenience polar coordinates, we write: $\mathbf{x} = (x_1, x_2) = (\rho, \theta) = (\|(x_1, x_2)\|, \arctan(x_2/x_1))$. We consider a basic PL estimator using the bases $(\phi_1(\mathbf{x}), \phi_2(\mathbf{x})) = (1, \rho)$, while the parametric space for GoB estimation is spanned by the basis functions $\psi_1(\theta), ..., \psi_{m_\theta}(\theta)$. The overall set of bases thus becomes

$$(\phi_1(\mathbf{x}), ..., \phi_m(\mathbf{x})) = (1, \rho, \psi_1(\theta), ..., \psi_{m_\theta}(\theta)),$$

where m_θ represents the number of bases we use for θ. We consider two sets of bases for the angular variable, specifically Fourier bases ($\psi_k^{(\mathcal{F})}(\theta)$) and Chebyshev polynomials ($\psi_k^{(\mathcal{C})}(\theta)$)

$$\psi_k^{(\mathcal{F})}(\theta) = \cos(k\theta), \quad \psi_k^{(\mathcal{C})}(\theta) = \cos(k \cos^{-1}(\theta)).$$

Fourier bases are widely used for function approximation [19], while Chebyshev polynomials are orthogonal polynomials that have been used in the context of antenna radiation pattern reconstruction [20]. In Fig. 1, some of the bases are plotted for both function types.

Given the dataset $\mathcal{D}$, the matrix $\boldsymbol{\Phi}$ takes the form

$$\boldsymbol{\Phi} = \begin{bmatrix} 1 & \rho_1 & \psi_1(\theta_1) & \dots & \psi_{m_\theta}(\theta_1) \\ \vdots & & \vdots & & \vdots \\ 1 & \rho_N & \psi_1(\theta_N) & \dots & \psi_{m_\theta}(\theta_N) \end{bmatrix}.$$

A good value for the hyperparameter m_θ can be learned from the data by cross-validation. Clearly, to limit the estimator complexity, m_θ shall be kept as small as possible. Simulation results for the selection of m_θ are discussed in Section IV.

C. Hyperparameters learning

The set of model hyperparameters is $\boldsymbol{\mathcal{P}} = \{\sigma, \lambda, d_c\}$. In what follows, we denote the matrix $\mathbf{A}$ of equation (8) by $\mathbf{A}(\boldsymbol{\mathcal{P}}) = \mathbf{A}_{\boldsymbol{\mathcal{P}}}$ to underline its dependence on $\boldsymbol{\mathcal{P}}$. The basic approach is to exploit (6) to set up a maximum marginal likelihood (ML) estimation procedure, i.e., the hyperparameters maximize the total probability where the shadowing process is integrated out. In particular, plugging equation (6) into the likelihood function, omitting terms not depending on $\boldsymbol{\mathcal{P}}$, one gets [26]

$$L_1(\boldsymbol{\mathcal{P}}; \mathbf{y}) = -\frac{1}{2}\log(|\mathbf{A}_{\boldsymbol{\mathcal{P}}}|) - \frac{1}{2}\mathbf{y}^T \mathbf{P}(\mathbf{A}_{\boldsymbol{\mathcal{P}}})\mathbf{y}, \tag{9}$$

where

$$\mathbf{P}(\mathbf{A}_{\boldsymbol{\mathcal{P}}}) = \mathbf{A}_{\boldsymbol{\mathcal{P}}}^{-1} - \mathbf{A}_{\boldsymbol{\mathcal{P}}}^{-1}\boldsymbol{\Phi}(\boldsymbol{\Phi}^T \mathbf{A}_{\boldsymbol{\mathcal{P}}}^{-1}\boldsymbol{\Phi})^{-1}\boldsymbol{\Phi}^T \mathbf{A}_{\boldsymbol{\mathcal{P}}}^{-1}, \tag{10}$$

where $\boldsymbol{\Phi}$ is as in (8). To learn the hyperparameters one then needs to maximize (9) over $\boldsymbol{\mathcal{P}}$. This method is known to be biased because of the loss in the degrees of freedom from estimating $\hat{\mathbf{w}}$ [26]. To compensate for this bias, an alternative approach is to consider not only the shadowing function as a zero-mean Gaussian process, but also the coefficients w_k as random, by modelling them as zero-mean Gaussian random variables with variance a and rewriting γ of (3) as

$$\tilde{\gamma}(\mathbf{x}) = \sum_{k=1}^{m} w_k \phi_k(\mathbf{x}) + \delta(\mathbf{x}),$$

where $\delta(\mathbf{x}) \sim \mathcal{GP}(0, K_{\boldsymbol{\mathcal{P}}}(\mathbf{x}, \mathbf{x}'))$, and $\mathbf{w} \sim \mathcal{N}(\mathbf{0}, a\mathbf{I})$, $\mathbf{w} = [w_1, ..., w_m]$. If $\hat{\gamma}(\mathbf{x})$ is the optimal least squares solution to the estimation problem, defining $\tilde{\gamma}_a(\mathbf{x}) = \mathbb{E}[\tilde{\gamma}(\mathbf{x})|y_1, ..., y_N]$, we have that (see [25] for a proof), $\lim_{a\to\infty} \tilde{\gamma}_a(\mathbf{x}) = \hat{\gamma}(\mathbf{x})$ for any fixed $\mathbf{x}$. For a finite, we get the data covariance matrix as

$$\tilde{\mathbf{K}}_{\boldsymbol{\mathcal{P}}}^{(a)} = \mathbb{E}[\mathbf{y}\mathbf{y}^T] = a\boldsymbol{\Phi}\boldsymbol{\Phi}^T + \mathbf{A}_{\boldsymbol{\mathcal{P}}}.$$

We can then learn the hyperparameters by maximizing the standard log-likelihood with the obtained covariance matrix

$$L_2^{(a)}(\boldsymbol{\mathcal{P}}; \mathbf{y}) = -\frac{1}{2}\mathbf{y}^T(\tilde{\mathbf{K}}_{\boldsymbol{\mathcal{P}}}^{(a)})^{-1}\mathbf{y} - \frac{1}{2}\log|\tilde{\mathbf{K}}_{\boldsymbol{\mathcal{P}}}^{(a)}|. \tag{11}$$

As we take the limit over a, there exists a closed form expression for the resulting covariance matrix, in particular (see [25], (1.5.12)), we have

$$\lim_{a\to\infty} (\tilde{\mathbf{K}}_{\boldsymbol{\mathcal{P}}}^{(a)})^{-1} = \mathbf{P}(\mathbf{A}_{\boldsymbol{\mathcal{P}}}), \tag{12}$$

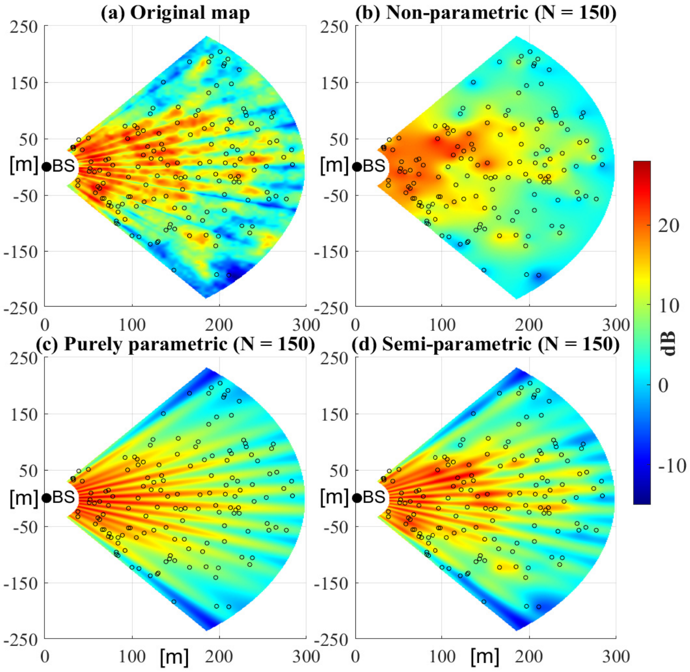

Fig. 2: Comparison of estimated maps for $N = 150$ measurement points (black circles) for an antenna array configuration with $n = 16$ beams.

where $\mathbf{P}(\mathbf{A}_{\boldsymbol{\mathcal{P}}})$ is defined in equation (10). The likelihood function obtained plugging (12) into (11) can be rewritten as

$$\begin{aligned} L_2(\boldsymbol{\mathcal{P}}; \mathbf{y}) &:= \lim_{a\to\infty} L_2^{(a)}(\boldsymbol{\mathcal{P}}; \mathbf{y}) \\ &= L_1(\boldsymbol{\mathcal{P}}; \mathbf{y}) - \frac{1}{2}\log|\mathbf{\Phi}^T \mathbf{A}_{\boldsymbol{\mathcal{P}}}^{-1} \mathbf{\Phi}|, \end{aligned} \tag{13}$$

which is equivalent to the so-called restricted maximum likelihood (REML). In [27], REML was proposed to perform hyperparameters learning for REM estimation, but in that work a small number of basis functions was used and only to capture the path loss effect. Furthermore, REML and ML were not compared and no numerical results were provided. Differently, in Section IV we provide a detailed numerical performance analysis for the considered hyperparameters learning strategies.

IV. Results

In this section, we assess the effectiveness of the proposed techniques in reconstructing REMs in a massive MIMO sector.

While the results shown were obtained with $d_c = 25$m, that is a typical value for the shadowing in urban environments, similar results were also attained with $d_c = 10$m and $d_c = 15$m, other typical values for the shadowing correlation distance. The other hyperparameters are set to $\lambda = 6$dB and $\sigma = 10^{-2}$. The choice of m_θ was made through cross-validation via parametric estimation - thus assuming the kernel function to be unknown - from a set of $N = 250$ measurement points. A good choice turned out to be $m_\theta = 50$.

In Fig. 2, we show the original radio map along with those estimated using three different approaches: (a) is the original map, (b) is the map obtained by restricting the parametric part of the estimator to the PL. This approach is referred to as *non-parametric*, as the GoB effect is entirely captured by means of non-parametric estimation. Map (c) is obtained by only relying on *parametric* estimation for both PL and GoB, where the latter is estimated via Fourier bases. Map (d) is obtained using the proposed *semi-parametric* regression method, where Fourier bases are used as described in Section III-A.

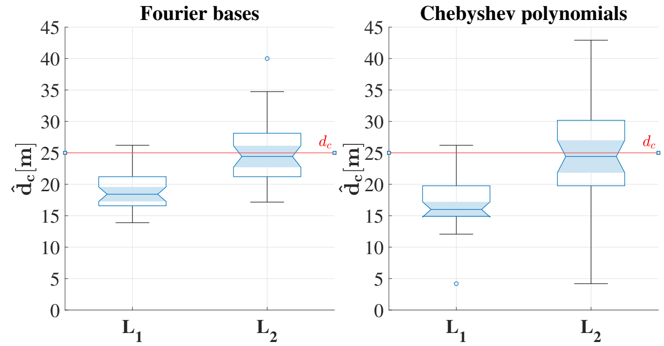

Fig. 3: Comparison of the hyperparameters learning strategies illustrated in Sec. III-C for the estimation of d_c. Results are shown for an antenna array configuration with $n = 16$ beams. The red line denotes the true correlation distance used to simulate the shadowing process, $d_c = 25m$.

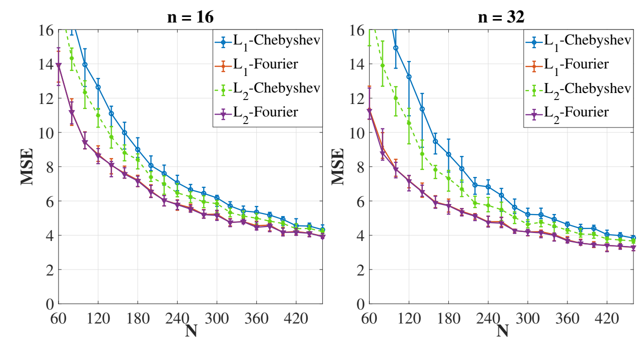

Fig. 4: MSE performance vs number of measurement points, N. The two semi-parametric estimation approaches (Fourier and Chebyshev) are compared, together with hyperparameters learning strategies. Results for $n = 16$ (left) and $n = 32$ (right) antenna beams are shown.

In Fig. 3, we show the results of the two hyperparameters learning strategies described in section III-C for the most relevant hyperparameter, d_c. To optimize L_1 and L_2, we iterate along possible values of the hyperparameters, considering a sufficiently small granularity in their domain sets, and compute the values of the function in the considered domain points. From the obtained grid we obtain an estimate of the maximizing tuple of hyperparameters. The box plots display the median, first and third quartiles, minima, maxima and outliers. For this graph, we executed $p = 40$ experiments in which $N = 200$ measurement points were randomly selected according to a uniform spatial distribution. The results demonstrate the improvement provided by L_2 in terms of learning accuracy, and also confirm that L_1 is biased.

In Fig. 4 and 5, we evaluate the map estimation accuracy

This article has been accepted for publication in a future issue of this journal, but has not been fully edited. Content may change prior to final publication. Citation information: DOI 10.1109/LWC.2021.3132458, IEEE Wireless Communications Letters

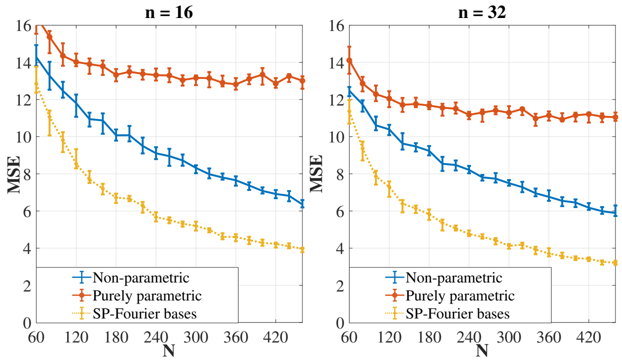

Fig. 5: MSE estimation performance vs number of measurement points, N. Results for $n = 16$ (left) and $n = 32$ (right) antenna beams are shown. SP stands for semi-parametric estimation.

in terms of Mean Squared Error (MSE) against the number of measurement points, N. For each choice of N, we executed $p = 40$ experiments and plotted the average MSE and the median confidence interval by randomly selecting the test points in unmeasured locations.

In Fig. 4, we compare the two basis functions (called Chebyshev and Fourier for brevity) and the hyperparameters learning strategy (L_1 vs L_2) for $n = 16$ and $n = 32$ antenna beams. For each experiment (a point in the plot), the learned hyperparameters (see Fig. 3) are used to define the kernel function. The results indicate that the Fourier basis provides the best accuracy. Furthermore, while using L_1 in place of L_2 provides a worse performance for Chebyshev, the difference is minimal for Fourier.

Finally, in Fig. 5 we compare the Fourier-based semi-parametric method against two competing strategies: the *non-parametric* and the *purely parametric* approaches, which were respectively used to obtain Figs. 2-(b) and 2-(c). The proposed method ("SP-Fourier bases" in the figure) achieves the best estimation accuracy for all the considered values of N.

V. Conclusion and Future Work

In this letter we studied crowdsourcing-based REM construction in a massive MIMO system through intensive simulation. Future research includes the study of the effectiveness of the proposed approach with datasets built upon real-world measurement campaigns and the extension of the setup to realistic 5G cellular systems like, e.g., urban and vehicular scenarios, including mobility and multiple base stations.

References

[1] H. Abou-zeid, H. S. Hassanein, and S. Valentin, "Optimal predictive resource allocation: Exploiting mobility patterns and radio maps," in *2013 IEEE Global Communications Conference (GLOBECOM)*, 2013, pp. 4877–4882.

[2] A. C. Suarez Rodriguez, N. Haider, Y. He, and E. Dutkiewicz, "Network optimisation in 5G networks: A radio environment map approach," *IEEE Transactions on Vehicular Technology*, vol. 69, no. 10, pp. 12 043–12 057, 2020.

[3] M. Hoffmann, P. Kryszkiewicz, and A. Kliks, "Increasing energy efficiency of massive-MIMO network via base stations switching using reinforcement learning and radio environment maps," *Computer Communications*, vol. 169, pp. 232–242, 2021.

[4] K. Sato, K. Suto, K. Inage, K. Adachi, and T. Fujii, "Space-frequency-interpolated radio map," *IEEE Transactions on Vehicular Technology*, vol. 70, no. 1, pp. 714–725, 2021.

[5] S. Bi, J. Lyu, Z. Ding, and R. Zhang, "Engineering radio maps for wireless resource management," *IEEE Wireless Communications*, vol. 26, no. 2, pp. 133–141, 2019.

[6] K. Katagiri and T. Fujii, "Radio environment map updating procedure considering change of surrounding environment," in *2020 IEEE Wireless Communications and Networking Conference Workshops (WCNCW)*, 2020, pp. 1–6.

[7] V.-P. Chowdappa, C. Botella, J. J. Samper-Zapater, and R. J. Martinez, "Distributed radio map reconstruction for 5G automotive," *IEEE Intelligent Transportation Systems Magazine*, vol. 10, no. 2, pp. 36–49, 2018.

[8] L. S. Muppirisetty, T. Svensson, and H. Wymeersch, "Spatial wireless channel prediction under location uncertainty," *IEEE Transactions on Wireless Communications*, vol. 15, no. 2, pp. 1031–1044, 2016.

[9] Y. Teganya and D. Romero, "Data-driven spectrum cartography via deep completion autoencoders," in *ICC 2020 - 2020 IEEE International Conference on Communications (ICC)*, 2020, pp. 1–7.

[10] K. Suto, S. Bannai, K. Sato, K. Inage, K. Adachi, and T. Fujii, "Image-driven spatial interpolation with deep learning for radio map construction," *IEEE Wireless Communications Letters*, vol. 10, no. 6, pp. 1222–1226, 2021.

[11] M. Pesko, T. Javornik, L. Vidmar, A. Košir, M. Štular, and M. Mohorčič, "The indirect self-tuning method for constructing radio environment map using omnidirectional or directional transmitter antenna," *EURASIP Journal on Wireless Communications and Networking*, vol. 15, no. 50, 2015.

[12] L. Bolea, J. Pérez-Romero, and R. Agustí, "Received signal interpolation for context discovery in cognitive radio," in *2011 The 14th International Symposium on Wireless Personal Multimedia Communications (WPMC)*, 2011, pp. 1–5.

[13] E. Björnson, L. Sanguinetti, H. Wymeersch, J. Hoydis, and T. L. Marzetta, "Massive MIMO is a reality—what is next?: Five promising research directions for antenna arrays," *Digital Signal Processing*, vol. 94, pp. 3–20, 2019.

[14] J. Palacios, N. González-Prelcic, and J. Widmer, "Managing hardware impairments in hybrid millimeter wave MIMO systems: A dictionary learning-based approach," in *2019 53rd Asilomar Conference on Signals, Systems, and Computers*, 2019, pp. 168–172.

[15] T. Iye, K. Tsuda, A. Tanibayashi, and Y. Fujii, "Evaluation of RF device error factors on the beam directivity of a uniform linear array antenna," *IEICE Communications Express*, vol. 9, no. 11, pp. 547–552, 2020.

[16] M. Eberhardt, P. Eschlwech, and E. Biebl, "Investigations on antenna array calibration algorithms for direction-of-arrival estimation," *Advances in Radio Science*, vol. 14, pp. 181–190, 2016.

[17] M. E. Eltayeb, T. Y. Al-Naffouri, and R. W. Heath, "Compressive sensing for millimeter wave antenna array diagnosis," *IEEE Transactions on Communications*, vol. 66, no. 6, pp. 2708–2721, 2018.

[18] F. Harrou and Y. Sun, "Statistical monitoring of linear antenna arrays," *Engineering Science and Technology, an International Journal*, vol. 19, no. 4, pp. 1781–1787, 2016.

[19] G. Konidaris, S. Osentoski, and P. Thomas, "Value function approximation in reinforcement learning using the Fourier basis," in *Twenty-fifth AAAI conference on artificial intelligence*, 2011.

[20] Z. Du, J. I. Moon, S.-s. Oh, J. Koh, and T. K. Sarkar, "Generation of free space radiation patterns from non-anechoic measurements using Chebyshev polynomials," *IEEE Transactions on Antennas and Propagation*, vol. 58, no. 8, pp. 2785–2790, 2010.

[21] A. Grassi, G. Piro, G. Boggia, M. Kurras, W. Zirwas, R. SivaSiva Ganesan, K. Pedersen, and L. Thiele, "Massive MIMO interference coordination for 5G broadband access: Integration and system level study," *Computer Networks*, vol. 147, pp. 191–203, Dec. 2018.

[22] S. Martiradonna, A. Grassi, G. Piro, and G. Boggia, "Understanding the 5G-air-simulator: A tutorial on design criteria, technical components, and reference use cases," *Computer Networks*, vol. 177, p. 107314, 2020.

[23] ITU-R, "Guidelines for Evaluation of Radio Interface Technologies for IMT-Advanced," Technical Report M.2135, 2008.

[24] 3GPP, "Study 3D Channel Model for LTE," 3rd Generation Partnership Project, Technical Specification 36.873, 01 2018, version 12.7.0.

[25] G. Wahba, *Spline models for observational data*. SIAM, 1990.

[26] A. E. Gelfand, P. Diggle, P. Guttorp, and M. Fuentes, *Handbook of spatial statistics*. CRC press, 2010.

[27] K. Sato and T. Fujii, "Kriging-based interference power constraint: Integrated design of the radio environment map and transmission power," *IEEE Transactions on Cognitive Communications and Networking*, vol. 3, no. 1, pp. 13–25, 2017.